Design and characteristics of DBR-laser-based environmental sensors

Yuri Beregovski *, Oliver Hennig, Mahmoud Fallahi, Francisco Guzman, Rosalie Clemens, Sergio Mendes, Nasser Peyghambarian

Optical Sciences Center, University of Arizona, Tucson AZ 85721, USA

Abstract

This paper reports on the development of a new laser-based chemical sensor. The optical sensor is based on the modification of the resonant cavity of a distributed-Bragg-reflector (DBR) laser. Part of the cavity (phase section and/or DBR grating) is covered by a sensitive layer that changes its refractive index as a result of interaction with a given chemical. This produces the change of optical cavity length, resulting in the lasing frequency shift. The results of modeling and preliminary experiments proving the concept of chemical sensing are presented. © 1998 Elsevier Science S.A. All rights reserved.

Keywords: Chemical sensors; Environmental monitoring; DBR lasers; External cavity

1. Introduction

There is an increasing need for high sensitivity, compact, low-cost and real-time sensors. Detection and identification of various liquids and gaseous species is required in the areas of semiconductor manufacturing, process control and environmental monitoring. Currently, mass spectrometers [1–3] and Fourier transform infrared (FTIR) systems [4] are the most widespread schemes for detection of low concentrations of chemicals. Contemporary mass spectrometers have relative sensitivity in the range of parts per million (ppm) in mobile versions [1], and below 1 part per trillion for stationary devices [2], with a detection limit of 10^{-18} mole [3]). However, as mass spectrometers require sample placement into the vacuum chamber, they are not real-time devices. FTIR sensors have been successfully used as environmental and biochemical sensors due to the simple optical scheme (compared to classical spectrometers). Mobile FTIR systems weighing 50 kg and consuming 100 W of electric power have been described [4]. However, these systems, like mass spectrometers, do not provide real-time on-line response.

The development of integrated optical components and the advances of fiber-optic devices over the past few years have opened a wide range of possible miniature sensor designs [5–8]. Most optical sensors have three major components: source of the coherent light (typically laser diode), chemically sensitive element and the detection system. Most integrated optical sensors are based on the change of the real or imaginary part of the refractive index of a sensitive material, which is within the penetration depth of the evanescent field, in the presence of a chemical in question. Fiber optic sensors are usually built on the principle of evanescent wave absorption in the medium surrounding the optical fiber [5 − 7], or the interferometric principle [8] detecting the slight changes of refractive index in the presence of chemicals. The scheme with the Mach–Zehnder interferometer is currently the most popular. One branch is affected by the chemical to be measured, while the other provides a reference phase. These sensors have the sensitivity comparable to the low-end mass spectrometers, providing real-time operation.

In this article, we present a new detection technique where the sensitive element is part of a resonant optical cavity to enhance the sensitivity. This technique uses the lasing wavelength shift of a distributed-Bragg-reflector (DBR) laser as a result of the change in optical

---

* Corresponding author.

cavity length caused by the refractive index change of the sensitive material. The same type of sensor can also be used to measure temperature and strain, since a change of these parameters will also induce a change of optical path length of the resonator. By using commercially available components, we expect this sensor to be low-cost and suitable for mass production. It also makes it possible to employ sensor arrays to detect many different chemicals at the same time.

In Section 2, the general concept of the sensor is presented, with a theoretical model for two types of sensor (monolithic and external cavity). The general characteristics of the sensor are presented for different designs. In Section 3, the experimental results for our DBR laser sensor are presented. Section 4 presents the concluding remarks about the proposed sensors.

2. Chemical sensing

2.1. General concept

In our detection scheme, the DBR laser is used as a chemical sensor (Fig. 1). Phase sections (Fig. 1(a)) or phase sections and grating (Fig. 1(b)) of the sensing laser are covered with a layer sensitive to the chemical in question. The action of the chemical produces refractive index change in the sensitive layer, thus changing the effective index of the section. As a result, the lasing frequency of the affected laser changes by a fraction determined by the concentration of the chemical (detailed analysis is supplied below). The second laser in both cases serves as a reference source. The reference laser has the same response to other environmental
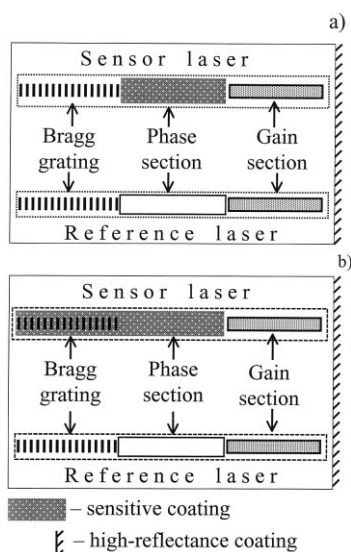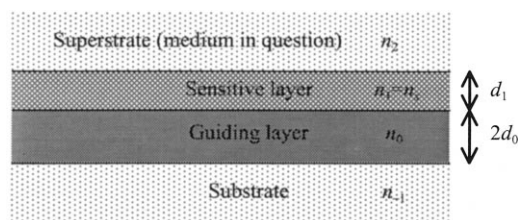

Fig. 2. Four-layer waveguide structure for chemical detection.

factors (first of all temperature) but not to the given chemical. Thus, the difference in lasing frequencies of the sensitive and reference lasers is used to measure the concentration of the chemical.

In a DBR laser, the lasing occurs if the gain compensates losses for at least one cavity mode. This mode lies within the bandwidth of the Bragg grating. If this condition is fulfilled for several modes, the one with the largest difference of gain and losses is dominant due to mode competition, thus producing single-mode operation. The lasing frequency is thus determined by:

$$v = q\frac{c}{2L},\tag{1}$$

where q is an integer number corresponding to the lasing mode, c is the speed of light, L is the optical length of the cavity. Thus, by changing the optical cavity length (for example, by changing the effective refractive index of some part of the cavity), lasing frequency can be changed accordingly. This allows use of part of the cavity (called phase section) as a frequency selective element for fine tuning within the bandwidth of Bragg grating. The same principle can be used for environmental sensing. For this purpose, the frequency selective element of the laser (Bragg grating and/or phase section) is coated with a sensitive polymer and immersed in the medium (Fig. 2). The presence of chemicals causes the change of the refractive index of the cladding. As a result, the effective index of the coated section of the cavity also changes, as does the optical length of the cavity [9,10]. Thus, the frequencies corresponding to cavity modes change, so that the lasing mode shifts within the peak of Bragg grating reflectance (Fig. 3).

2.2. Theoretical analysis

The resolution of the DBR laser-based sensor is limited by the resolvable frequency shift. The major limitation of this resolvable shift is the linewidth of the laser. The advantage of DBR lasers as sensors is the possibility of obtaining a narrow linewidth in a monolithic or a simple external cavity laser. The linewidth of a DBR laser is approximately given by [13]:

Fig. 1. DBR laser-based sensor with coated phase sections (a) or phase sections and gratings (b).

$$\Delta v = \frac{hv}{8\pi P}\left(\frac{L_a}{L_a + L_e}\right)^2\left(\frac{c}{n_{eff}}\right)^2 (g_{th} - \alpha_a)g_{th}(1 + \alpha^2)n_{sp},$$

(2)

where P is output power; L_a and L_e are the active and effective passive waveguide lengths, respectively; g_{th} is the threshold gain; c is the velocity of light; n_{eff} is the effective refractive index; α is the linewidth enhancement factor; α_a is the loss coefficient in the active region; and n_{sp} is the spontaneous emission factor. The threshold gain g_{th} is, in turn, calculated by the formula:

$$g_{th} = \alpha_a + \frac{1}{L_a}\left[L_e\alpha_e + \frac{1}{2}\ln\left(\frac{1}{R_f R_r}\right) + \ln\left(\frac{1}{C}\right)\right],$$

(3)

where R_f and R_r are the front and rear side reflectances, respectively and C is the power coupling efficiency between the active and passive sections.

To obtain the narrow linewidth, good power coupling between active and passive sections, low modal losses and long cavity (relatively to the length of gain section) are therefore necessary. Efficiency of lens coupling in the case of external cavity may be 30–70% (for monolithic lasers, power coupling between active and passive sections may be 95% or more). Low modal losses are achieved by using multiple-quantum-well (MQW) gain layer and, in the case of monolithic lasers, regrowth technology for grating regions (though the losses in fiber gratings are still much lower). This, together with improved layer structure and Bragg reflector efficiency, has allowed to reduce the linewidth from 3.2 [14] to less than 100 kHz for monolithic DBR lasers [15,16]. Short-term linewidth of less than 300 kHz has already been achieved for commercial external cavity semiconductor lasers, with further improvement possible. This, together with the possibility of separating the semiconductor gain section from the harsh environment, makes the external cavity design very attractive for proposed sensors. Due to the narrow linewidth of DBR lasers, small changes of the effective index and, correspondingly, small concentrations of chemicals may be accurately detected.

A simple external cavity design is based on the sensitive element and Bragg grating formed on the ridge waveguide. This design provides good mode matching with the semiconductor gain section and allows manufacturing of an array of sensors with multi-chemical detection capability. Another way is to use single-mode fiber Bragg grating as feedback and phase section. In this case, part of the fiber has to be polished close to the core (D-shape) and coated with sensitive material. This technique allows to use simple procedures like polishing and dip-coating for sensor fabrication.

There are two possible ways of evaluating the frequency change. One of them is monitoring of the frequency shift with the Fabry–Perot interferometer that has a typical resolution of several megahertz. The second technique is based on heterodyne detection. In this approach, outputs of the sensor and reference lasers are combined and sent to the optical detector connected with a microwave spectrum analyzer. Since the heterodyne technique can provide a resolution determined by the linewidth of used sources, it takes advantage of the full sensitivity of the proposed sensors.

Apart from the geometrical dimensions and the laser linewidth, the key parameter of the proposed sensors is $\partial n_{eff}/\partial n_s$, where n_s is the refractive index of the sensitive layer (Fig. 2). The evaluation of this parameter may be made using the equations for guided-mode eigenvalues [17,18] (Appendix A)

$$\frac{\partial n_{eff}}{\partial n_s} = \frac{n_s}{n_{eff}}\Gamma_s,$$

(4)

where Γ_s is the field confinement factor for the sensitive layer.

The results of numerical modeling of frequency shift are presented in Fig. 4. Fig. 4(a) is related to a fully integrated (monolithic) version. Fig. 4(b) is related to an external-cavity structure based on planar waveguides. Typical values for the key parameters are assumed (Table 1). The present calculations are made in the infinite slab approximation. However, the similar results can be obtained for other guiding configurations.

The graphs show that covering both gratings and phase sections with sensitive layer produces a proportionally larger frequency shift. However, the layer structure on the top of Bragg grating has to be very uniform in order to preserve the shape of frequency-response curve of the gratings (otherwise the frequency selectivity of the scheme will be affected). Thus, a detection scheme with only phase sections coated may be more feasible technologically, since the effect of phase section is determined by the change of optical length integrated over the phase section and does not require high unifor-
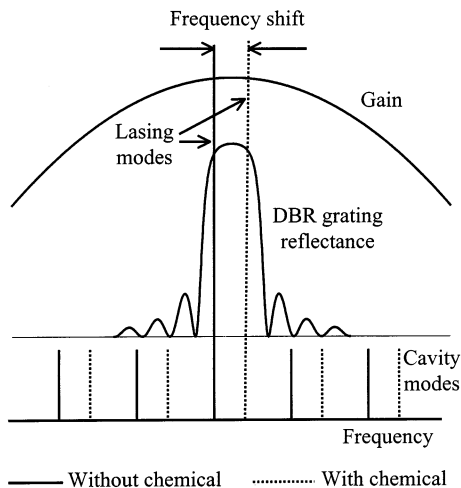

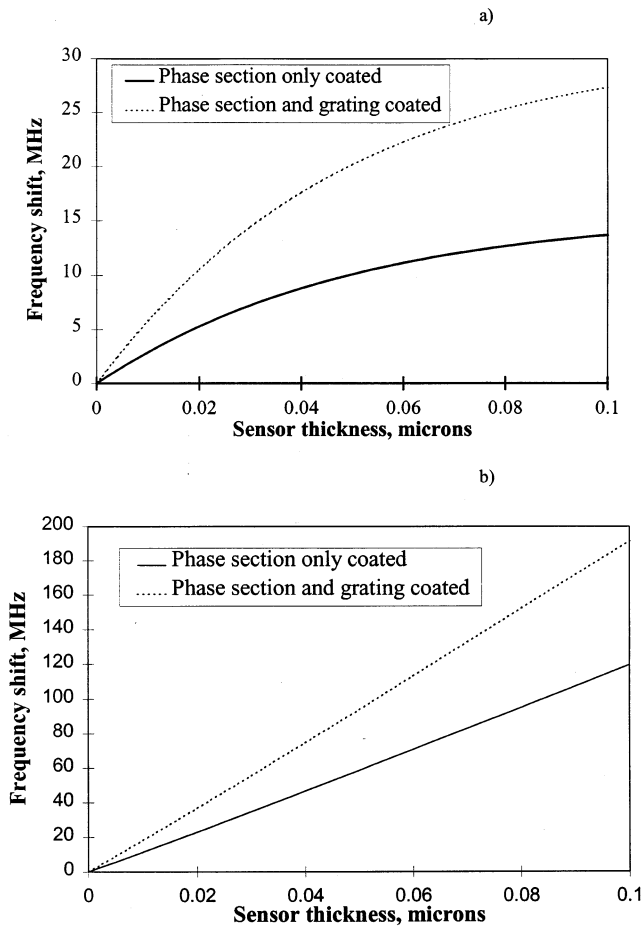Fig. 3. Diagram of the DBR lasing mode and frequency shift.

Fig. 4. Frequency shift vs. sensitive layer thickness for an on-chip (a) and external-cavity configuration (b).

Table 1
Parameters of the on-chip and external-cavity DBR-laser-based sensors used in modeling

	Monolithic version	External cavity
Guiding layer thickness (μm)	0.3	1
Guiding layer refractive index	3.4	1.6
Protective cladding thickness (μm)	0.02	–
Sensitive layer thickness (μm)	0.1	0.1
Sensitive layer refractive index	1.46	1.46
Substrate refractive index	3.1	1.46
Gain section length (mm)	0.3	0.4
Phase section length (mm)	0.3	10
Bragg grating effective length (mm)	0.3	10
Sensor refractive index change	10^{-4}	10^{-4}
Wavelength (μm)	1.55	1.55
Power confinement in sensitive layer	0.0145	0.0176

quency shifts may be obtained by choosing materials with larger range of refractive index change. The optimum choice of the material for sensitive layer, therefore, has to be made for each case separately.

An optimum configuration of the sensor requires the maximum ratio of frequency shift caused by a certain concentration of the chemical to laser linewidth, i.e. the maximum ratio of $\partial n_{eff}/\partial n_s$ to Δv. Such an optimum is achievable due to the fact that both $\partial n/\partial n_s$ and losses increase with the confinement in the sensing layer Γ_s; however, the frequency shift increases with Γ_s linearly, while Δv presents a second-power polynomial dependence. Thus, an optimum confinement always exists and is defined by the condition:

$$\frac{d}{d\Gamma_s}\left(\frac{\partial n_{eff}/\partial n_s}{\Delta v}\right) = 0 \qquad (5)$$

mity. These graphs allow to make an estimation of resolvable refractive index change of the sensitive layer (assuming a resolvable frequency shift equal to the laser linewidth). Considering a 1-MHz linewidth of the external cavity design, the resolvable refractive index change would be better than 10^{-6}.

In the case of a monolithic structure, the power confinement in the sensitive layer strongly depends on the thickness of the protective cladding (which is necessary for technological reasons and higher reliability). The frequency shift versus refractive index change of the sensitive layer was modeled for different thickness of the protective layer using the same parameters as before (Fig. 5).

Power confinement in the sensitive layer depends on the refractive index of this layer (apart from the layer structure). The optical materials that may be used for this layer have refractive indices between 1.4 and 2.5. The results show that higher refractive indices produce larger confinement and, consequently, larger frequency shifts (Fig. 6). On the other hand, higher refractive index of the outer (sensitive) layer means higher losses, first of all due to surface scattering. Also, larger fre-
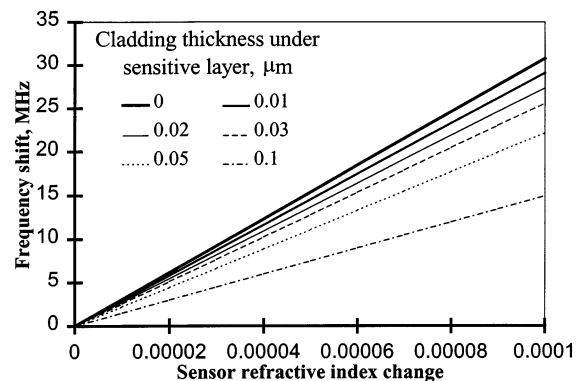

Fig. 5. Frequency shift vs. refractive index change of the sensitive layer for different thickness of protective cladding.
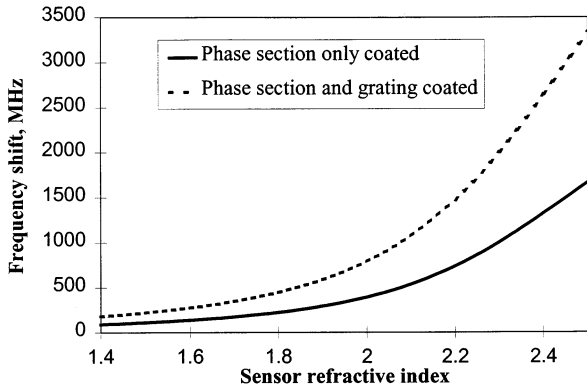
Fig. 6. Frequency shift vs. refractive index of the sensitive layer (other parameters are the same as in Fig. 4(a)).

This gives the optimum value for Γ_s:

$$\Gamma_s = \frac{\sqrt{Q(Q + \alpha_a L_a)}}{L_e \alpha_s}, \tag{6}$$

where

$$Q = \frac{1}{2} \ln\left(\frac{1}{R_1 R_2}\right) + \ln\left(\frac{1}{C}\right) \tag{7}$$

α_s is loss coefficient in the sensitive layer, the rest of variables are the same as in Eqs. (1) and (2). Other layers of the passive section are assumed to be low-loss.

The key challenges are to create a sensitive element with the desired optical and chemical characteristics as well as to enable the sensor to detect sufficient small changes in the effective refractive index of the sensitive element, induced by the species in question. As a goal of detectable changes, we aim to achieve a resolution higher than Mach–Zehnder-based sensors. Mach–Zehnder sensors are based on measuring the relative phase shift between the measuring arm and sensitive arm: A change in the effective refractive index of the sensitive element causes the optical length of the sensitive arm to change, thus resulting in a relative phase shift between both arms. The minimum detectable refractive index change of the sensitive layer in a Mach–Zehnder interferometer is:

$$\Delta n_s = \frac{\lambda \delta}{2\pi L_s \frac{\partial n_{eff}}{\partial n_s}} \tag{8}$$

where δ and λ are the minimum detectable phase shift and light wavelength, respectively; L_s is the length of the sensitive section which may be made equal to the length of the interferometer. Other parameters in Eq. (8) are the same as before.

According to [11,12], phase shifts as low as $\delta = (1–2) \times 10^{-3}$ radian can be measured. Thus, the resolution of a Mach–Zehnder-based sensor may be compared to that of a DBR laser-based sensor (Fig. 7). The graph shows lines of equal resolution. The resolution of the

Mach–Zehnder-based sensor increases with increasing length of the sensitive element (which may be made equal to the total length of the interferometer). In the case of the DBR-laser-based sensor, the resolution improves with increasing ratio of sensitive section length to the total cavity length and does not depend on the actual size of the sensitive element. From the graph it is clear that a resolvable shift in frequency < 1 MHz has to be achieved to obtain a resolution comparable to the one of Mach–Zehnder devices. The resolution of the DBR laser-based sensor can be improved by having the sensitive element change the refractive index of the cladding at the distributed Bragg reflector in addition to the change in optical path length of the phase section. This both increases the total change of the optical path length and provides the change of the reflectivity peak of the frequency selective element in the same direction.

3. Experimental results

3.1. Chemical sensor

For the proof of concept, a fiber grating external cavity DBR laser was selected. We have used matching pairs of gratings and laser diodes in the 1550-nm region. The gain section consisted of a Fabry–Perot InGaAsP/InP multiple quantum well (MQW) laser diode mounted p-side up on the heat sink. The front facet of laser diode and cleaved facet of the optical fiber grating were AR-coated to reduce the reflectance to less than 0.1%. Fibers were butt-coupled to the semiconductor gain sections using the fiber positioner. The fiber gratings used in the experiments had peak reflectances within 88–95% and bandwidth of 0.1–1 nm according to the specifications.
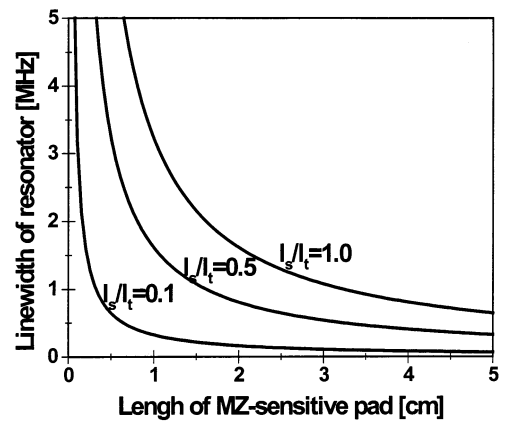

Fig. 7. Comparison of an external-cavity DBR-laser-based chemical sensor with a Mach–Zehnder interferometer (layer structure of the sensor is the same as in the interferometer).
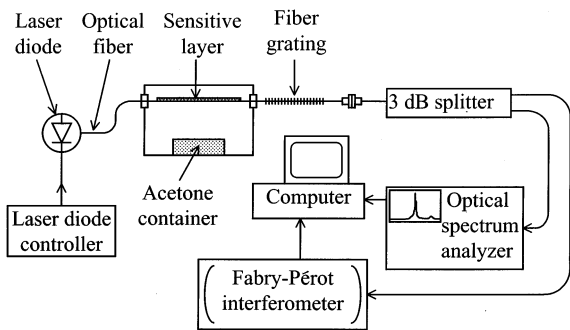
Fig. 8. Scheme of the chemical sensor set-up.

Fig. 9. Emission spectrum of the external-cavity DBR laser with fiber grating recorded by an optical spectrum analyzer with 0.8 Å resolution.

An experimental set-up (Fig. 8) was used for detection of acetone vapors in the air. It was based on an external-cavity DBR laser scheme using fiber DBR grating with 1550 nm peak wavelength. The fiber containing the 95% reflectance, 1-nm-bandwidth grating was butt-coupled to the gain section (the coupling efficiency was measured at 12%). Prior to the butt-coupling, a section of the fiber adjacent to the grating (phase section) was polished close to the core (with power output control as a criterion of polishing depth) and dip-coated with a polymer sensitive to acetone and toluene. This section was placed into the enclosure where a container with acetone could be placed (so as to allow the build-up of vapor concentration within 5–10 s). The other end of the fiber was used to couple light into the Fabry–Perot interferometer. After achieving the maximum laser power output by positioning the fiber, an acetone container was placed in the enclosure containing the sensitive section, and the latter was closed. During the vapor build-up, the frequency shift could be observed visually on the interferometer display. The reversibility of the polymer response allowed to make a series of measurements on the same sample. The response time of the sensor is determined by the response time of the sensitive layer, since the response of the laser to an index change is very fast. In a separate experiment [19], the response of this sensitive layer was measured to be on the order of seconds, with full reversibility after termination of the influx of a chemical.

The typical spectrum of a fiber-based DBR laser is shown in Fig. 9. Here a distributed Bragg reflector with a FWHM = 0.14 nm and a peak reflectivity of 88% has been used. The center wavelength of the semiconductor gain as well as of the reflectivity peak was at ~1538 nm.

A side-mode suppression better than 34 dB has been achieved. Using a scanning Fabry–Perot interferometer, a linewidth 3–5 MHz and short-term instability of 26 MHz (RMS) were measured. The most probable cause of frequency instability was mechanical instability of the experimental set-up.
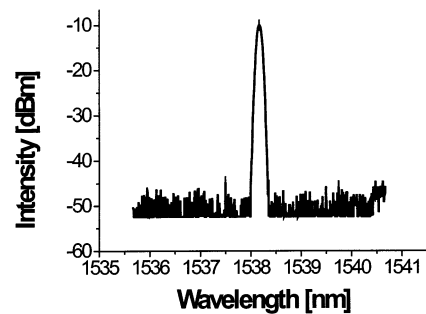
The results of the measurements are shown in Fig. 10. They indicate an ~130-MHz frequency shift as a result of the presence of acetone vapors, with return to the initial frequency after exposure to acetone. The group of peaks in each spectrum indicates several lasing modes resolvable by the Fabry–Perot interferometer (Fig. 9). The entire group of lasing modes shifts simultaneously under the action of acetone.

Two different configurations of the sensitive element (with coated grating and coated phase section) were tested. The results presented above (for coated phase section) have the RMS error due to instability approximately half of that produced by the scheme with coated gratings. This may be attributed to the change of grating frequency response caused by the non-uniformity of polishing and coating the grating section.

3.2. Temperature sensitivity

The sensitivity of DBR lasers to temperature is important for two reasons. Firstly, the frequency shift due to typical changes of ambient temperature is much larger than the above-listed frequency shift resulting from chemicals. This shift is usually large enough to be detected by classical spectral analyzers. Thus, in the
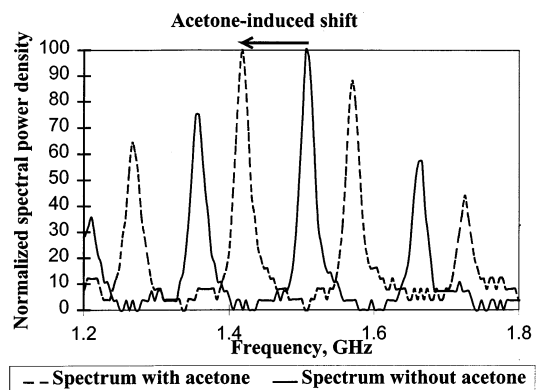

Fig. 10. Frequency shift of a DBR laser in the presence of acetone vapors measured with Fabry–Perot interferometer.
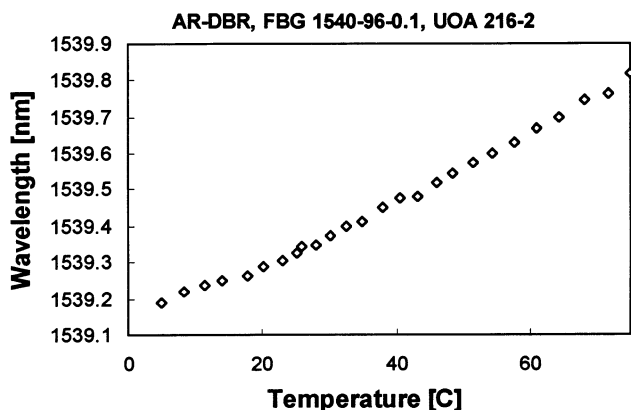
Fig. 11. Temperature dependence of fiber-grating DBR lasing wavelength.

case of chemical sensors, this shift has to be either compensated (as in differential scheme) or accurately accounted for. Secondly, due to the same reason of large magnitude, the temperature-induced frequency shift may be used for direct temperature measurements. In the case of an external-cavity fiber grating DBR laser, the fiber may be used in harsh environments.

The theoretical background of temperature measurements is supplied in Apendix B. The experiment was carried out using the AR-coated semiconductor laser ($\lambda = 1525$ nm at room temperature before coating) and a single-mode optical fiber with Bragg grating of a nominal wavelength 1540 nm. The cleaved fiber was butt-coupled to the laser and its output measured with HP-70950B optical spectrum analyzer. The temperature of the Bragg grating was varied by placing it onto a Peltier element (producing the temperature changes up to 70°). During the experiment the grating was protected from environmental influences other than controlled temperature changes (such as air streams.). The actual temperature was controlled by a thermoelectric sensor placed on the Peltier element adjacent to the fiber grating.

A wavelength shift of 0.01 nm °C^{-1} for the Bragg wavelength was verified in the experiment between room temperature and 75°C. Experimental data are shown in Fig. 11.

Therefore, the thermal sensitivity of DBR lasers shows the advantage of a differential detection scheme proposed for chemical sensing. Such a scheme would not have the temperature-related instability. Also, the magnitude of the wavelength changes allows to detect changes using simple and inexpensive spectral techniques (particularly because these changes occur in the vicinity of the wavelength known in advance).

4. Conclusions

The frequency change of DBR lasers as a result of environmental changes has been used for chemical and temperature detection. A single-channel scheme (without a reference source) allows to detect large concentrations of vapors, while a differential scheme may have the potential sensitivity equal to that of a 10-cm or larger Mach–Zehnder interferometer. The external-cavity schemes (with waveguides on a glass or SiO$_2$ substrate) provide an overall higher sensitivity when used with polymer sensitive layers. The analysis shows that, unlike the passive fiber-optic sensors, the DBR-based sensors have an optimum value of power confinement in the sensitive layer. This optimum value is primarily the function of loss coefficient of the sensitive material and the length of the sensitive section. The experimental results prove the concept of DBR-laser-based chemical sensing.

Appendix A. Evaluation of $\partial n_{eff} / \partial n_s$ for 3- and 4-layer structures

The eigenequations for the qth mode are [17,18]:

$$2h_0 d_0 - \varphi_{+0} - \varphi_{-0} - q\pi = 0, \qquad (A1.1)$$

where φ_{+0} and φ_{-0} are half-phase shifts on the bottom and top boundaries of the guiding level, respectively. For a simple 4-layer structure used for chemical detection (Fig. 2), the equations for these half-phase shifts are the following:

$$\varphi_{-0} = \tan^{-1}\left(\frac{p_{-1}}{h_0}\right); \quad \varphi_0 = \tan^{-1}\left(\frac{p_1}{h_0}\tanh\psi_1\right)$$
$$(A1.2)$$

$$\psi_1 = p_1 d_1 + \tanh^{-1}\left(\frac{p_2}{p_1}\right);$$

$$h_0 = k_0\sqrt{n_0^2 - n_{eff}^2}; \quad p_i = k_0\sqrt{n_{eff}^2 - n_i^2}$$
$$(i = -1, 1, 2)$$

$$k_0 = 2\pi / \lambda_0$$

assuming that $n_0 > n_{eff} > n_{-1,1,2}$. The sensitive layer in this scheme is number 1, thus $n_s = n_1$.

Consequently, for each guided mode, the following is true:

$$\frac{\partial}{\partial n_i}(2h_0d_0 - \varphi_{+0} - \varphi_{-0}) = 0. \tag{A1.3}$$

A simple evaluation may be made for a 3-layer structure, with the refractive indices of substrate, guiding layer and superstrate n_{-1}, n_0, and $n_1 = n_s$, respectively. Guiding layer thickness remains to be $2d_0$. For this structure:

$$2h_0d_0 - \varphi_{-0} - \varphi_{+0} - q\pi = 0; \tag{A1.4}$$

$$\varphi_{-0} = \tan^{-1}\left(\frac{p_{-1}}{h_0}\right); \quad \varphi_{+0} = \tan^{-1}\left(\frac{p_1}{h_0}\right)$$

Other parameters are defined in Eq. (5).

For this structure, the following equation for $\partial n_{\text{eff}}/\partial n_s$ may be obtained:

$$\frac{\partial n_{\text{eff}}}{\partial n_s} = \frac{n_s}{n_{\text{eff}}}\frac{h_0^2}{p_1(h_0^2 + p_1^2)}\frac{1}{2d_0 + \dfrac{1}{p_1} + \dfrac{1}{p_{-1}}} \tag{A1.5}$$

This is equivalent to the following expression:

$$\frac{\partial n_{\text{eff}}}{\partial n_s} = \frac{n_s}{n_{\text{eff}}}\Gamma_s \tag{A1.6}$$

This is similar to the formulae obtained in [20,21] from the perturbation theory.

Appendix B. Temperature and strain sensitivity

Temperature and strain influence on the fiber result in a Bragg wavelength shift of

$$\Delta\lambda_B = 2n_{\text{eff}}\Lambda\Bigg(\left\{1 - \left(\frac{n_{\text{eff}}^2}{2}\right)[P_{12} - v(P_{11} + P_{12})]\right\}\varepsilon$$
$$+ \left[\alpha + \frac{dn/dT}{n_{\text{eff}}}\right]\Delta T\Bigg) \tag{B2.1}$$

where the factor $(n_{\text{eff}}^2/2)[P_{12} - v(P_{11} + P_{12})]$, including Pockel's coefficients of the stress–optic tensor, Poisson's ratio and the fiber's refractive index, equals ~ 0.22. ε represents the applied strain and α the thermal expansion coefficient. ΔT is the temperature change of the grating [22].

With constant temperature, the normalized strain response for a 1.3 μm- grating can be expressed as

$$\frac{1}{\lambda_B} \cdot \frac{\delta\lambda_B}{\delta\varepsilon} = 0.78 \cdot 10^{-6}\mu\varepsilon^{-1} \tag{B2.2}$$

This value gives a wavelength shift of roughly 1 nm per 1000 με.

The wavelength shift due to temperature changes is mainly dependent on the change of the refractive index and thermal expansions of the fiber material. For silica fibers the normalized wavelength shift for constant strain is

$$\frac{1}{\lambda_B} \cdot \frac{\delta\lambda_B}{\delta T} = 6.67 \cdot 10^{-6}\,^{\circ}\text{C}^{-1} \tag{B2.3}$$

which gives a wavelength shift of 0.008–0.01 nm °C^{-1} within the examined spectral region [22].

References

[1] V.T. Kogan, A.D. Kazanskii, et al., Portable mass spectrometer for environmental monitoring, Pribory Tekhnika Eksp. 38 (1) (1995) 159–165.

[2] Y. Takao, Y. Kanda, A system for measurements of sub-parts-per-trillion helium in solids, Rev. Sci. Instrum. 67 (1) (1996) 198–202.

[3] W.A. Bryden, R.C. Benson, et al., The tiny TOF spectrometer for chemical and biological sensing, Johns Hopkins APL Tech. Dig. 16 (3) (1995) 296–309.

[4] H. Rainer et al., Remote sensing of air pollution by mobile Fourier-transform spectroscopy: modeling and first results of measurements, Optical Remote Sensing Applications to Environmental and Industry Problems, Houston, TX, 6–8 April, 1992, pp. 67–75.

[5] R. Krska, R. Kellner, et al., Fiber optic sensor for chlorinated hydrocarbons in water based on infrared fibers and tunable diode lasers, Appl. Phys. Lett. 63 (1993) 1868–1870.

[6] M.H. Maher, M.R. Shahriari, A Fiber Optic Chemical Sensor for Measurements of Groundwater pH, J. Test. Eval. 21 (5) (1993) 448–452.

[7] C. Egami, K. Takeda, et al., Evanescent-wave spectroscopic fiber optic pH sensor, Opt. Commun. 122 (1996) 122–126.

[8] Y. Liu, P. Hering, M.O. Scully, An integrated optical sensor for measuring glucose concentration, Appl. Phys. B 54 (1992) 18–23.

[9] S. Ten, M. Fallahi, N. Peyghambarian, Design of a novel semiconductor laser-based chemical sensor, Proc. SPIE 2763 (1996) 64–69.

[10] Y. Beregovski, S. Ten, S. Mendes, et al., In situ chemical detectors based on photonic devices, Proc. SPIE 3082 (1997) 76–82.

[11] B.J. Luff, J.S. Wilkinson, J. Piehler, et al., Integrated optical Mach–Zehnder biosensor, J. Lightwave Technol. 16 (4) (1998) 583–592.

[12] J. Dakin, B. Culshaw, Optical Fiber Sensors, vol. 4: Application, Analysis and Future Trends, Artech House, Boston, 1997.

[13] Y. Kotaki, H. Ishikawa, Spectral characteristics of a three-section wavelength-tunable DBR laser, IEEE J. Quantum Electron QE-25 (1989) 1340–1345.

[14] M. Takahashi, Y. Michitsuji, et al., Narrow spectral linewidth 1.5 μm GaInAsP/InP distributed Bragg reflector (DBR) lasers, IEEE J. Quantum Electron QE-25 (1989) 1280–1286.

[15] T. Kunii, Y. Matsui, et al., Narrow linewidth (85 kHz) operation in long cavity 1.5 μm-MQW laser, Electron. Lett. 27 (9) (1991) 691–692.

[16] G.M. Smith, J.S. Hughes, et al., Very narrow linewidth asymmetric cladding InGaAs-GaAs ridge waveguide distributed Bragg reflector lasers, IEEE Photonics Technol. Lett. 8 (4) (1996) 476–478.

[17] Y.-F. Li, J.W.Y. Lit, General formulas for the guiding properties of a multilayer slab waveguide, JOSA 4 (4) (1987) 671–677.

[18] Y.-F. Li, J.W.Y. Lit, Effective thickness, group velocity, power flow, and stored energy in a multilayer dielectric planar waveguide, JOSA 7 (4) (1990) 617–635.

[19] K.M. Grace, K. Shrouf, S. Honkanen, et al., Waveguide Zeeman interferometry for thin-film chemical sensors, Electron. Lett. 33 (19) (1997) 1651–1652.

[20] O. Parriaux., in: O. Wolfbeis (Eds.), Fiber Optic Chemical Sensors and Biosensors, CRC Press, Boca Raton, FL, 1991, vol. 1, pp. 111–192.

[21] A.W. Snyder, J.D. Love, Optical Waveguide Theory, Chapman and Hall, NY, 1983.

[22] A.D. Kersey, et al., Fiber grating sensors, J. Lightwave Technol. 15 (8) (1997) 1442–1462.